Published in Physica E: Low-dimensional Systems and Nanostructures 7, issues 1-2, 25-28, 2000
which should be used for any reference to this work

Edge- and surface-emitting 10.1 μm quantum cascade distributed feedback lasers

Daniel Hofstetter[a, *], Jérôme Faist[a], Mattias Beck[a], Antoine Müller[a], Ursula Oesterle[b]

[a] *University of Neuchâtel, Institute of Physics, 1 Rue A.-L. Breguet, Neuchâtel, CH 2000, Switzerland*
[b] *Swiss Federal Institute of Technology, Physics Department, PHB Ecublens, Lausanne, CH 1015, Switzerland*

Abstract

We present measurement results on high-power low-threshold quantum cascade-distributed feedback lasers emitting infrared radiation at 10.16 μm. A lateral current injection scheme allowed the use of a strongly coupled surface grating without metal coverage and epitaxial re-growth. Although this design resulted in a simplified processing, the fabrication of high-performance edge- and surface-emitting devices was demonstrated. For the edge-emitting laser, we used a standard first-order grating with a period of 1.57 μm, and for the surface emitter, a second-order grating with a period of 3.15 μm was used. Maximal output powers in excess of 200 mW at 85 K and 70 mW at 300 K were achieved for both configurations. The threshold current densities at 85 K (300 K) were 1.85 kA/cm^2 (5.4 kA/cm^2) and 2.1 kA/cm^2 (5.6 kA/cm^2) for edge and surface emitters, respectively.

Keywords: Quantum cascade lasers; Distributed feedback lasers; Surface emission; Lateral current injection

Quantum cascade (QC) lasers are very promising light sources for environmental sensors in the mid-infrared spectral region [1–3]. Most of these applications require the use of single-mode light sources; be they edge- or surface-emitters. This requirement can be accomplished by using a distributed feedback (DFB) laser [4–6]. In order to achieve standard edge-emission, we fabricated devices with a first-order grating, while for the surface-emitters, a second-order grating was used [7]. Although DFB lasers have obvious performance benefits, they usually suffer from the fact that epitaxial re-growth is necessary to complete the structure after grating fabrication. As has been recently demonstrated, one can use a lateral current injection scheme in order to fabricate a strongly coupled, low-loss grating without epitaxial re-growth [5]. These devices have a waveguide with a semiconductor lower cladding and air forming the top cladding. The heavily n-doped InGaAs cap layer, which serves as a host layer for the grating, is highly conducting to allow lateral current injection and -distribution throughout the device. This results in both a high coupling coefficient of the grating and a relatively high net gain of the laser; thus

* Corresponding author. Tel.: +41-32-718-3545; fax: +41-32-718-2901.
E-mail address: daniel.hofstetter@iph.unine.ch (D. Hofstetter)

it potentially allows the fabrication of short devices with a low threshold current.

Growth of this material was based on molecular beam epitaxy (MBE) of lattice-matched InGaAs/InAlAs layers on top of an n-doped InP (Si, 2×10^{17} cm^{-3}) substrate. The growth process started with the lower waveguide layers (InGaAs, Si, 1×10^{17} cm^{-3}, total thickness 1.5 μm), proceeded with an active region (thickness 1.75 μm) and was finished by a thicker set of upper waveguide layers (thickness 2.2 μm) and a 0.7 μm thick highly n-doped cap layer on top. This cap layer was also the host layer for the grating, as mentioned earlier. The active region, which thus formed the central part of the waveguide, consisted of 35 super-lattice periods; those were alternating n-doped funnel injector regions and undoped triple quantum well active regions. The laser transition in the latter was diagonal, similar to that described in Ref. [8]. The layer sequence of the structure, in nanometers, starting from the injection barrier, is as follows: 3.9/**1.0**/3.8/**1.2**/3.7/**1.5**/3.9/**1.7**/4.0/**4.2**/3.1/**0.9**/6.4/ **1.0**/6.0/**2.8** nm. $In_{0.52}Al_{0.48}As$ layers are in bold, $In_{0.53}Ga_{0.47}As$ layers are in roman, and n-doped layers (Si 2.5×10^{17} cm^{-3}) are underlined.

The fabrication of these DFB lasers was based on holographically defining a grating with either 1.57 μm (first-order grating) or 3.15 μm period (second-order grating, $n_{\text{eff}} = 3.22$), and wet chemical etching of the grating in a $H_2SO_4/H_2O_2/H_2O$ solution to a depth of 0.6 μm (etch rate 100 nm/sec). We used a 488 nm Ar-ion laser and a 90° corner reflector mounted on a rotational stage for the grating exposure. The grating lines run along the dove-tail direction of the crystal in order to achieve non-rectangular profile and to obtain a sufficiently high first-order Fourier component. This is quite critical for the performance of the surface-emitting laser because a symmetric rectangular second-order grating contains no first-order Fourier component. In addition, the combination holography/wet etching for the fabrication of the grating involves a high risk of obtaining a duty cycle which is considerably smaller than 50%. Since a small duty cycle reduces the average refractive index and therefore also the overlap factor of the grating layer, the coupling coefficient becomes small, resulting in an even poorer efficiency of the grating.

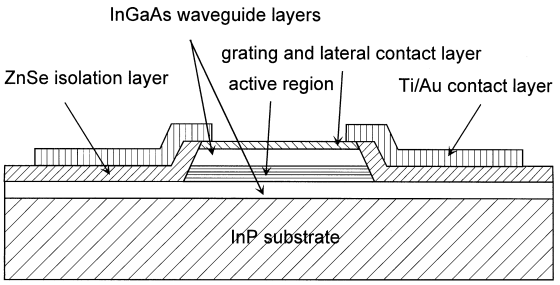

Fig. 1. Schematic cross-section through the waveguide of a DFB laser. The top metal contact covers only a small fraction on both shoulders of the waveguide.

Standard processing techniques were used to define ridge waveguides with a width of 35–55 μm (etch depth 4.5 μm, $HBr/HNO_3/H_2O_2$, etch rate 800 nm/min) and a length of 1–1.5 mm [5]. 300 nm of ZnSe served as an electrical passivation layer and Ti/Au (10/400 nm) was used as top contact metal. Thinning, back contacting (Ge/Au/Ag/Au, 12/27/50/100 nm), and cleaving completed the processing. As shown by the schematic cross-section in Fig. 1, the contact metal covered only the edges (about 5 μm on each side) of the ridge to avoid large absorption losses in the waveguide, but still to allow lateral current injection. The devices, whose facets were left uncoated, were mounted ridge side up on copper heat sinks and operated at different temperatures between 85 and 300 K. The samples were then placed into a temperature-controlled N_2 flow cryostat. The light from the facet or the grating of the DFB QC laser was collected by f/0.8 optics and fed into a high-resolution Fourier transform spectrometer (Nicolet-type Magna-IR 860), where we detected it by using a liquid nitrogen-cooled HgCdTe detector. For the measurement of *L–I* curves, we measured the intensity with a calibrated 500×500 μm^2 room temperature HgCdTe detector. For both types of lasers, the current pulses were 100 ns long, and a pulse repetition frequency of 5 kHz was used for all temperatures. A typical *L–I* and *I–V* curve of the first-order DFB laser are presented in Fig. 2. For a 1.2 mm long and 45 μm wide laser, a maximal output power of 230 mW at 85 K and 80 mW at room temperature was seen. The device emitted single-mode radiation for all temperatures and power levels. The threshold current was 1 A at 85 K and increased to 2.9 A at

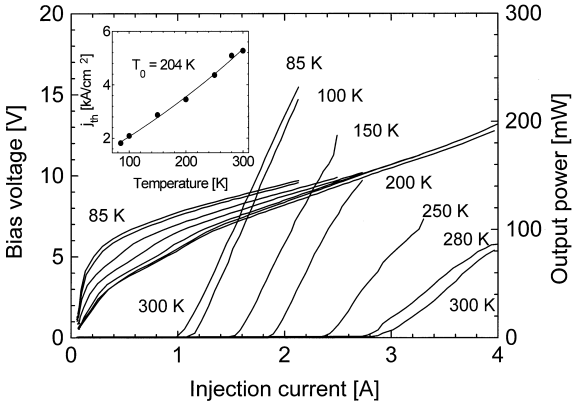

Fig. 2. *L–I* and *I–V* curve of a first-order DFB laser measured at different temperatures between 85 and 300 K. The inset shows how the threshold current changes with increasing temperature.

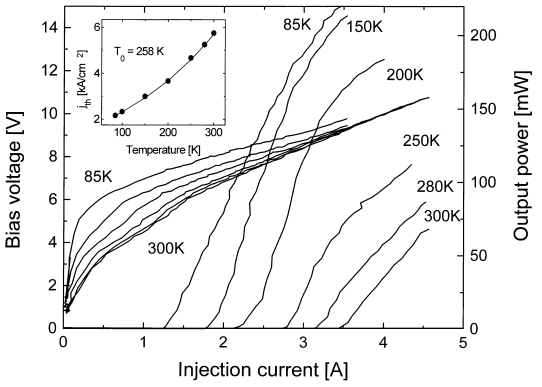

Fig. 3. *L–I* and *I–V* curve of a surface-emitting second-order DFB laser measured at temperatures between 85 and 300 K. The inset shows the threshold current change with increasing temperature.

300 K, corresponding to threshold current densities of 1.85 and 5.4 kA/cm^2, respectively. Edge emission *L–I* and *I–V*-curves of a 55 μm wide and 1.125 mm long surface-emitting device are shown in Fig. 3. At low temperatures, we observed a threshold current of 1.3 A and a maximum output power of 210 mW from the facet. The slope efficiency at this temperature was 105 mW/A and a threshold current density of 2.1 kA/cm^2 was determined. At room temperature, we obtained 70 mW optical output power from the facet, with a slope efficiency of 70 mW/A. However, the threshold current increased to 3.45 A (threshold current density of 5.6 kA/cm^2), and an operating voltage of 10.5 V was seen. From the increase in

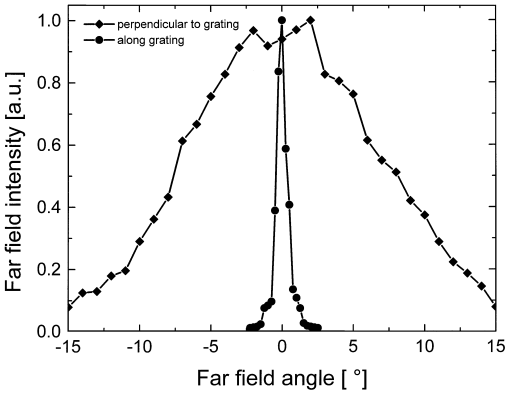

Fig. 4. Far field distribution of a surface-emitting second-order DFB laser in the directions both parallel and perpendicular to the waveguide.

threshold current, we were able to derive a characteristic temperature T_0 of 204 K for the first-order DFB laser and 258 K for the surface-emitting DFB laser.

In Fig. 4, we present the vertically emitted far-field distribution of the surface-emitter in both directions. In the direction along the waveguide, we observed, due to the wide aperture and the Bragg reflection, a very narrow far-field angle of about 1° (FWHM), whereas in the other, perpendicular direction, the far-field angle was equivalent to the one observed at the corresponding direction of the facet, namely about 14° (FWHM). Such a far field distribution will facilitate coupling into a micro-optical sensor system in the respect that a cylindrical lens instead of an aspherical one will be sufficient to achieve a parallel laser beam.

Spectral measurements below lasing threshold allowed a relatively precise measurement of the Bragg reflector's stop-bandwidth, the value obtained was 2.6 cm^{-1} for the first-order and 1.1 cm^{-1} for the second-order DFB laser. From these figures, we determined the coupling coefficients of the grating to be $\kappa = \Delta\lambda\pi n_{\text{eff}}/\lambda^2 = 28$ cm^{-1} and 12 cm^{-1}, respectively. A relatively small free carrier absorption loss of 12 cm^{-1} was calculated for both devices, whereas a laser utilizing our standard waveguide design with a 2.2 μm thick InAlAs/InGaAs upper cladding layer and a metal-covered grating would suffer from a waveguide loss of 30 cm^{-1}. In addition, the refractive index contrast would be reduced by almost two orders of magnitude.

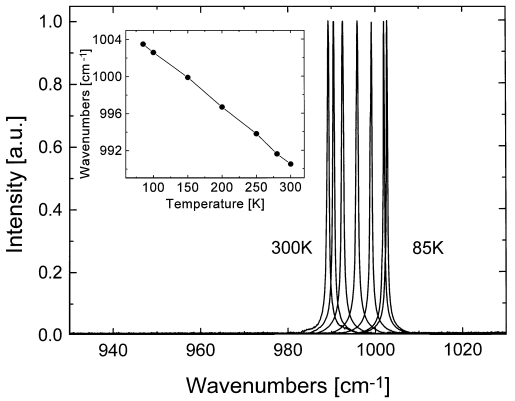

Fig. 5. Optical emission spectra of a second-order DFB laser measured at different temperatures between 85 and 300 K. The inset shows the linearity of the temperature tuning.

Finally, Fig. 5 shows the lasing spectra of the second-order DFB laser at temperatures between 85 and 300 K. We determined the line width to be of the order of 0.3 cm^{-1}, which corresponds to the resolution limit of our experimental set-up. The emission wavelength at 85 K was 1003 cm^{-1}, at room temperature, it decreased to 989 cm^{-1}. The luminescence peak was found in the vicinity of 990 cm^{-1} for all temperatures. The temperature-tuning coefficient of the lasing peak was constant over the entire temperature range, and its magnitude was $1/\lambda \times \Delta\lambda/\Delta T = 6.1 \times 10^{-5}$ K^{-1} ($\Delta\nu/\Delta T = -0.06$ cm^{-1}/K). These numbers are consistent with what has been reported in the literature [6].

In conclusion, we have shown device results for both first-order and second-order DFB QC lasers operating at 10.1 μm. These DFB lasers function without upper cladding layer, the grating is therefore directly exposed to air. Current injection is accomplished laterally through the grating layer; this design avoids large waveguide losses due to metal absorption. At room temperature, both types of lasers emitted in excess of 70 mW optical power through the facet, the second-order device an additional 18 mW from the grating. The corresponding numbers for 85 K were > 200 and 60 mW for facet and grating emissions, respectively. Pulsed threshold current densities of 5.4 kA/cm^2 (5.6 kA/cm^2) and 1.85 kA/cm^{-2} (2.1 kA/cm^2) for the first- (second-) order DFB laser were seen. For the surface-emitting laser, the far-field angle in the narrow direction along the waveguide was of the order of 1°, in the direction perpendicular to the waveguide, we observed a far field angle of 14°.

Acknowledgements

We would like to thank Stéphane Blaser, and Antoine Müller for their advice during processing, electrical and spectral measurements on these samples, and the Swiss National Science Foundation and the Science Foundation of the European Community under contract BRITE/EURAM project UNISEL (No. CT97-0557) for their financial support.

References

[1] J. Faist, F. Capasso, D.L. Sivco, A.L. Hutchinson, A.Y. Cho, Science 264 (1994) 553.
[2] J. Faist, F. Capasso, C. Sirtori, D.L. Sivco, J.N. Baillargeon, A.L. Hutchinson, S.N.G. Cho, A.Y. Cho, Appl. Phys. Lett. 68 (1996) 3680.
[3] C. Sirtori, J. Faist, F. Capasso, D.L. Sivco, A.L. Hutchinson, A.Y. Cho, Appl. Phys. Lett. 68 (1996) 1745.
[4] J. Faist, C. Gmachl, F. Capasso, C. Sirtori, D.L. Sivco, J.N. Baillargeon, A.Y. Cho, Appl. Phys. Lett. 70 (1997) 2670.
[5] D. Hofstetter, J. Faist, A. Müller, M. Beck, U, Oesterle, Appl. Phys. Lett. 75 (1999) 665.
[6] C. Gmachl, F. Capasso, J. Faist, A.L. Hutchinson, A. Tredicucci, D.L. Sivco, J.N. Baillargeon, S.N.G. Chu, A.Y. Cho, Appl. Phys. Lett. 72 (1998) 1430.
[7] G.A. Evans, D.P. Bour, N.W. Carlson, J.M. Hammer, M. Lurie, J.K. Butler, S.L. Palfrey, R. Amantea, L.A. Carr, F.Z. Hawrylo, J.B. Kirk, S.K. Liew, W.F. Reichert, Appl. Phys. Lett. 55 (1989) 2721.
[8] J. Faist, C. Sirtori, F. Capasso, D.L. Sivco, J.N. Baillargeon, A.L. Hutchinson, A.Y. Cho, IEEE Photonics Technol. Lett. 10 (1998) 1100.